Predicting Water Sorption and Volume Swelling in Dense Polymer Systems via Computer Simulation

Henning Hörstermann,[†] Reinhard Hentschke,*[,†] Marc Amkreutz,[‡] Michael Hoffmann,[‡] and Martin Wirts-Rütters[‡]

Fachbereich Mathematik und Naturwissenschaften, Bergische Universität, D-42097 Wuppertal, Germany, and Fraunhofer Institute for Manufacturing Technology and Applied Materials Research, Wiener Strasse 12, D-28359 Bremen, Germany

Received: June 7, 2010; Revised Manuscript Received: November 17, 2010

Atomistic model structures of amorphous polyamide 6 (PA-6) and of an adhesive system consisting of the diglycidyl ether of bisphenol A (DGEBA) as epoxy resin and isophorone diamine (IPD) as a curing agent are generated. For the adhesive, we use a new approach for the generation of the cross-linked polymer networks. It takes into account the chemical reaction kinetics of the curing reaction and, therefore, results in more realistic network structures. On the basis of the corresponding model structures, the equilibrium water content and the swelling ratio of amorphous PA-6 and of the DGEBA+IPD networks are calculated via computer simulation for different thermodynamic conditions. A hybrid method is used combining the molecular dynamics technique with an accelerated test particle insertion method. The results are in reasonable agreement with experiments and, in the case of the PA-6 system, with results obtained via other computer simulation methods.

I. Introduction

Equilibrium sorption of small molecules in polymer networks is important in many applications of polymers, for example, membrane filtration, bonding agents, packings, and so forth. Estimating and predicting sorption from computer simulations is therefore of great practical use. Here, we are specifically interested in the equilibrium sorption of water in polymers and the volumetric changes of the polymer network due to swelling. For example, the swelling of an adhesive by water vapor in the surrounding air leads to deformation or displacement of the bonded parts. This is an unwanted effect in applications requiring high precision like optical or measuring systems.

Generation of Polymer Network Structures. A realistic model of the polymer network structure is an important prerequisite for the successful simulation of sorption and swelling. For the generation of realistic non-cross-linked systems with long polymer chains, various construction methods exist. One of the most well-established and widely used ones is the method of Theodorou and Suter.[1] Using their construction method, polymer structures and resulting properties, like, for example, diffusion of small molecules in the polymer, are usually well described (see e.g., refs 2−7). For cross-linked polymers, these methods are not adequate, especially for adhesive systems where the network forms via a curing reaction over a long time. Hence, the challenge when generating a realistic polymer structure of an adhesive is the correct description of the curing reaction. This requires a proper cross-linking scheme for the corresponding functional groups of the adhesive over the curing time, which can be in the range of seconds to weeks depending on the type of adhesive.

There are kinetic models describing the curing reactions of epoxy resins in detail yielding the degree of cross-linking and the epoxide conversion over time, taking into account effects like autocatalysis and diffusion control.[8−12] These methods require that the kinetic constants for all relevant reaction steps leading to new chemical species be known. More important, these methods do not yield an atomistic model structure of the polymer. On the other hand, atomistic simulations of reactions in general using semiempiric or ab initio methods are restricted to small system sizes. Force field methods are able to handle sufficiently large system sizes, but the description of the curing reactions is usually not covered by these methods.

Hence, nowadays, the state-of-the-art approach for the generation of an adhesive network in the case of amine-cured epoxies is, in general, as follows.[13−18] First, a non-cross-linked mixture of resin and curing agent with a given experimental ratio is generated and equilibrated via force-field-based molecular dynamics (MD), providing a starting structure for the generation of cross-linked structures. The next step is the analysis of the system regarding the distances of the corresponding reactive sites and the "manual" formation of new bonds if a conversion criterion, for example, a predefined reaction cutoff distance, is fulfilled. In some cases, the potential reactive sites are activated before cross-linking by breaking of the epoxy ring and removal of the hydrogens of the amine groups. In a last step, the final cross-linked state is equilibrated, which yields the cured adhesive.

Yarovsky and Evans[13] used an arbitrary cross-link cutoff of 6 Å as criterion in order to avoid excessive strain in the system, which is, of course, system-dependent. Wu and Xu[14,15] repeated the cross-linking of the reaction partners within a reaction cutoff distance range from 4 to 10 Å until the conversion was within the range of the experimental value of 93.7%. For such an approach, the necessary experimental data (conversion, density) must be available, but this is nevertheless macroscopic information providing no detail about the cross-linking on the atomic scale. In contrast, Fan and Yuen[16] generated a fully cured adhesive system with 100% degree of cross-linking. This is however unlikely under normal curing conditions because in

* To whom correspondence should be addressed. E-mail: hentschk@uni-wuppertal.de.
[†] Bergische Universität.
[‡] Fraunhofer Institute for Manufacturing Technology and Applied Materials Research.

10.1021/jp105210y © 2010 American Chemical Society
Published on Web 12/09/2010

the case of adhesives, a slow down of conversion occurs due to the cross-linking. Varshney et al.[17] repeated the formation of bonds until a predefined cross-linking limit was reached. They used four approaches with different assumptions regarding the reactivity of the primary and secondary amine and the cutoff distances. In particular, the choice of the cutoff was arbitrary and depended on the approach. Clancy et al.[18] used a range of degrees of cross-linking and moisture content to study the relationship between these structural parameters and the effects of hygrothermal aging on epoxies and thus generate typical generic epoxy systems for a parameter study.

All of the outlined approaches rely on more or less arbitrary distance criteria for the cross-linking or on a final conversion or density from experiment as a macroscopic fitting parameter. Thus, there is no reliable indication that the created network is realistic on the atomic scale because macroscopic quantities like density and conversion do not contain the necessary atomistic information, that is, the exact number of the various types of cross-links formed in the cured adhesive. Theoretically, there exist countless possible networks, all possessing the same degree of cross-linking and density but varying strongly in their number of primary, secondary, and tertiary amines. However, especially for the calculation of volume shrinkage, water sorption, and volume swelling, a realistic network structure is imperative. Thus, there is still need for a method able to generate more realistic atomistic structure models of adhesives. This can be achieved if the chemical reactivity of the adhesive's reactive species is taken into account on the atomic level, that is, the formation of bonds is based on reaction kinetics instead of a distance criterion. This new approach utilizing the combination of a kinetic model, based on data obtained from thermal analysis, and a force-field-based MD method will be introduced here for an adhesive system. This system consists of the diglycidyl ether of bisphenol A (DGEBA) as an epoxy resin and isophorone diamine (IPD), also known as 1-amino-3-aminomethyl-3,5,5-trimethylcyclohexylamine, as a curing agent and is cured at 296 K.

Water Sorption of Polymer Networks. Sorption of water by a polymer network reaches equilibrium once the chemical potential of water molecules inside of the polymer is equal to the chemical potential of water in the surrounding medium. In order to find the chemical equilibrium, we calculate the chemical potential of water in neat water and inside of the model polymer network already containing varying amounts of water. Comparing the results, we identify the water content for which the chemical potentials of water inside of the bulk liquid and the polymer network are equal. In addition, we estimate the equilibrium water content if the polymer is in contact with air at a given relative humidity instead of liquid water.

Calculating the chemical potential of small molecules like water inside of a polymer network via computer simulation is challenging. The commonly used test particle insertion method invented by Widom[19] and independently by Jackson and Klein[20] becomes increasingly inefficient at high densities. Numerous approaches try to circumvent this problem by modification of the test particle insertion method or by supplementing it with other methods like thermodynamic coupling parameter integration. In this work, we use an accelerated Widom method, which has already been used to calculate the chemical potential of bulk water[21] and of water in a model epoxy resin.[22] It counters the inefficiency of the test particle insertion method by using a grid search algorithm to identify regions inside of the network where insertions of test particles yield negligible contributions to the chemical potential. The standard Widom method is then used in the remaining regions only. Pandiyan, Brown, Neyertz, and van der Vegt[23] used a similar simulation method as the one used in this work to study the sorption of carbon dioxide and volume swelling for three fluorinated polyimides. They calculated the chemical potential of the carbon dioxide molecules by a variant of the excluded volume map sampling (EVMS) technique, a sampling method proposed by Deitrick, Scriven, and Davis,[24] that uses an approach similar to the accelerated Widom method. The EVMS method was also applied by Tamai, Tanaka, and Nakanishi[25] and Fukuda[26] to calculate the chemical potential of several small molecules, one of them water, in polymers. Another grid search algorithm for suitable regions for test particle insertions was used by Zanuy et al.[27] to simulate the solubility of various small penetrants in poly(α-alkyl-β-L-aspartate)s. Nick and Suter utilized a combination of Widom's test particle insertion method and thermodynamic coupling parameter integration[28] to compute the chemical potential of water in several polyamides[29] and other polymers.[30] They calculated the chemical potential of a water model without charges and scaled down size, that is, noble water, by Widom's test particle method and then used thermodynamic coupling parameter integration of the aforementioned parameters to estimate the chemical potential of the full water model. Van der Vegt and Briels[31] calculated the chemical potential of solvent molecules in a polymer system by introducing the strength of the interaction as an additional dynamical variable and compared their "extended ensemble molecular dynamics" method (EEMD) with thermodynamic integration. The standard Widom test particle method was applied also by Müller-Plathe to calculate the free energy of several gases in amorphous polypropylene[32] and by Lim, Tsotsis, and Sahimi to calculate the chemical potential of carbon dioxide and methane in polyetherimide.[33]

Another set of methods for direct simulation of equilibrium sorption and swelling uses the Gibbs ensemble, where two separate simulation boxes — one containing the polymer including the solvent and the other the solvent only — exchange volume and solvent particles. There are studies of the swelling of model polymer networks by different solvents where the solvent transfer is implemented using Monte Carlo methods[34−39] or MD.[40] De Pablo, Laso, and Suter[41] introduced a combination of the Gibbs ensemble method and a biased test particle insertion algorithm to estimate the solubility of alkanes in polymers, which allowed them to describe the sorption of pentane in polyethylene in good agreement with experiments. Sommer et al.[42,43] studied ideal athermal swelling of polymer networks using the bond fluctuation model on a 3D cubic lattice. The authors simulated the swelling of the network by moving it onto a larger lattice. Kenkare, Hall, and Khan[44] studied the swelling of hard chain polymer networks by a hard sphere solvent via a combined discontinuous molecular dynamics (DMD) and Monte Carlo simulation study. They used the DMD method to conduct the displacement and volume-change moves in a μPT Monte Carlo framework.

In this work, the developed hybrid method for the simulation of swelling is first tested for an "amorphous cell" polyamide 6 (PA-6) system, and the findings are compared to experimental results in the literature as a benchmark. Additionally, DGEBA+IPD networks are studied via computer simulation encompassing the identification and characterization of the chemical reactions important for the curing of the network, the generation algorithm for realistic network structures based on this information, and an atomistic simulation of the swelling of these networks by water via the hybrid method.

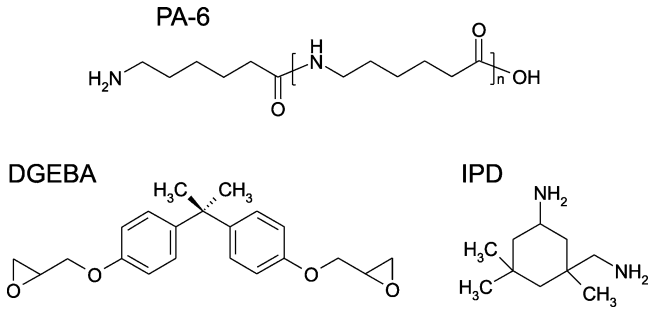

Figure 1. Chemical structures of the amorphous polyamide 6 (PA-6, top), the diglycidyl ether of bisphenol A (DGEBA, bottom left), and the isophorone diamine (IPD, bottom right).

The paper is structured as follows. Section II describes the method applied to create realistic models for polymer networks. Section III explains the algorithms used to calculate the chemical potential of water inside of the polymer networks and how the equilibrium water content is obtained based on simulation, and section IV describes the results for the two polymer systems studied here. Section V is the conclusion.

II. Generation of Polymer Network Structures

PA-6. Amorphous PA-6 model structures (see Figure 1) are generated via the Amorphous Cell module of the Materials Studio MS 4.4 software (Accelrys Software Inc.[45]). We note that the ultimate goal of this work is the application of the present approach to industrial bonds in order to estimate their water uptake under thermodynamically realistic conditions. Therefore, we decided to base much of the present work on widely used commercial and open-source software, available in most industrial materials research laboratories. It is consistent to use the same software for the generation of amorphous PA-6, which here serves a control purpose. Ten independent packing models are created to increase the statistical significance. The initial structures are relaxed using 10000 steps of MD and 1000 steps of energy minimization using the polymer consistent force field (PCFF).[46−52] van der Waals interactions are computed with an atom-based cutoff distance of 8.5 Å. Coulombic interactions are computed using a cell multipole method. The temperature control method is direct velocity scaling with a time step of 1 fs for the velocity Verlet algorithm. For the optimization, a conjugate gradient approach (Polak−Ribière) is applied. Cubic periodic cells possessing a side length of 20.52 Å and containing one polymer chain of PA-6 with 50 monomeric units (953 atoms) and a density of $\rho = 1.09$ g/cm^3 are created at 298 K. Subsequently, the constructed periodic cells are converted to be used as input for the LAMMPS molecular dynamics software[53] as provided by Sandia National Laboratories[54] for further simulation of the water sorption and volume swelling of PA-6.

At this point, we briefly address possible effects due to finite size. Basically, there are two types of finite size effects, those depending on the linear expanse of the simulation system and those depending on its overall volume. The former type of finite size effect occurs, for instance, in the context of critical phenomena (e.g., near-critical fluctuation correlation functions). However, it may also be observed in tightly meshed polymer networks due to its elastic entropy (a discussion is given by one of the present authors in ref 55). In the case of PA-6, the network is not tightly meshed, and no such effect is important. However, even for tightly meshed networks, as another model study shows,[38] the effects on sorption and separation are minor for the system size considered here (referring to the DGEBA+IPD polymer network).

The second type of finite size effects, which depend on the bulk material content rather than the linear system dimension, is more relevant in our case. One instance is the sufficient sampling of holes suitable for water insertion. Here, we like to point out that, in the case of PA-6 as well as in the case of DGEBA+IPD, we use 10 independently generated systems, which increases the effective (bulk) sizes of the polymer systems to 10^4 and 1.5×10^4 atoms, respectively. On the basis of the aforementioned work on competitive sorption in model polymer networks,[38] there are no significant finite size effects to be reckoned with at such system size (at least not in comparison to other sources of error). In particular, the consideration of 10 parallel smaller systems instead of a single large system has the advantage that possible bias problems during system construction are reduced.

DGEBA+IPD. For the adhesive system consisting of DGEBA and IPD (see Figure 1), the Amorphous Cell module of MS 4.4 is used for the construction of the non-cross-linked mixture of resin and curing agent. A near-stoichiometric mixture of 23 DGEBA molecules and 11 IPD molecules is used, resulting in a cubic periodic cell with a side length of 25.25 Å and an initial density of $\rho = 1.00$ g/cm^3 at 296 K (curing temperature) containing 1501 atoms. Again, 10 independent model structures are created for better statistics. All structures are relaxed using 1000 steps of MD and 100 steps of energy minimization using the PCFF force field. The summation methods for the nonbonded interactions, the temperature control method, the time step, and the optimization method are the same as those in the case of the amorphous PA-6. As before, the systems are converted to be used as input for LAMMPS for further investigation of the cross-linking reaction and the water sorption and swelling behavior.

The generation of the cross-linked systems is performed using the LAMMPS software and the PCFF force field. The nonbonded interactions are modeled via a 9−6 potential for van der Waals and a pairwise Coulomb interaction. For both interactions, a global cutoff of 12.0 Å is used, including a long-range van der Waals tail "correction" to the energy and pressure. The non-cross-linked mixture of resin and curing agent is equilibrated using a combination of *NVT* and *NpT* simulations at atmospheric pressure with a time step of 1 fs. The Nose−Hoover thermostat and barostat are used for temperature and pressure control, respectively.[56,57] Initially, a structure minimization using the conjugate gradient method (50 steps) is performed. Subsequently, a *NVT* MD with temperature increasing from 0 to 500 K during 100 ps followed by a *NVT* MD at 500 K for 200 ps is applied for an extensive mixing of the system at constant density. This is followed by a *NpT* MD at 500 K for 200 ps and a cooling from 500 to 296 K over 100 ps. Finally, a *NpT* MD at 296 K for 800 ps equilibrates the system at the target temperature. The last 400 ps are used as production run to obtain the density of the adhesive, $\rho = 1.044$ g/cm^3.

For the cross-linking based on the chemical reactivity of the different functional groups of the resin and curing agent, the following approach is applied. First, the relevant cross-linking reactions are identified. In this case, four reactions are considered to be important for the formation of the network because IPD possesses two different reactive amine groups which could react twice each, (i) the reaction of the 1-amino group with an epoxide followed by (ii) the reaction of the now secondary amine with another epoxy ring to form a ternary amine, (iii) the reaction of

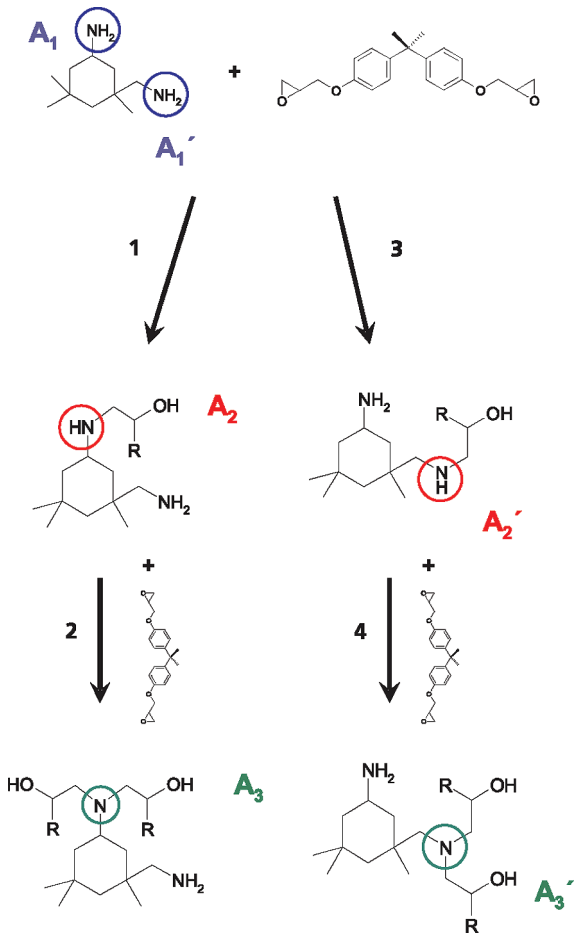

Figure 2. Division of the overall cross-linking reaction into two independent parallel reactions with two reaction steps each resulting in the formation of the species, that is, cross-linking sites A_2 and A_3 from the 1-amino group and A_2' and A_3' from the 3-aminomethyl group. The primary amines A_1 and A_1', secondary amines A_2 and A_2', and ternary amines A_3 and A_3' are highlighted.

the primary amine of the 3-aminomethyl group with an epoxide, and after that, (iv) the reaction of the now secondary amine with an epoxy group. It could be shown that the etherification reactions are negligible for curing at room temperature and that the reactivities of the two different amine functions are independent. Therefore, the overall cross-linking reaction can be divided into two independent parallel reactions with two reaction steps each (see Figure 2). For each of these steps, a modified Kamal equation[58] is used to determine the kinetic constants of the single reactions like activation energy, velocity constant, and autocatalytic constant using thermal analysis, that is, differential scanning calorimetry (DSC). Therefore, model reactions of DGEBA with model agents of IPD, possessing only one corresponding reactive amine function each, are investigated. Specifically, aminomethylcyclohexan, cyclohexylamine, and *N*-ethylcyclohexylamine are used as model agents for IPD. With the resulting kinetic constants, the reaction equations for the single model reactions are known. Finally, the overall curing reaction is fitted by the four single reactions according to the works of Flammersheim and Opfermann.[59,60] As a result, it can be shown that the reactivities of all four reactions are different, that is, the primary amines do not possess the same reactivity as the secondary ones for both parallel reactions. Furthermore, the reactivity of the amino group of the 3-aminomethyl is significantly higher than the one of the 1-amino group. In a last step, the reaction equations for the overall curing reaction are solved to calculate the concentrations over time of each species A_2, A_2', A_3, and A_3' (see Figure 3). This gives the information about how many primary, secondary, and tertiary amines exactly exist in the adhesive at each point of time and, thus, how many and which kind of cross-links have to be created. With this information, an atomistic model can be generated for any corresponding curing time desired, where the cross-linking is based on the reaction kinetics including autocatalysis, diffusion control, and filler effects. For more details, see Kolbe et al.[61] and further publications in preparation.

On the basis of the equilibrated non-cross-linked mixture, models for two kinds of cured adhesives are generated. One model, DGEBA/IPD, is constructed for the adhesive without fillers and without taking into account diffusion control according to the concentrations obtained from the corresponding kinetic modeling in Figure 3, top and middle. This serves later as an additional test system for the evaluation of the new approach to calculate the swelling behavior. The other model, DGEBA/IPD+FDC, is generated for the adhesive with fillers (F) and diffusion control (DC), beginning after a curing time of approximately 8 h and a conversion of 52% as obtained from DSC and rheology experiments. This is considered the realistic adhesive system. The addition of fillers is not taken into account explicitly because the size of the fillers used is too large to integrate them in the periodic supercell of the model. Hence, the model structure is intended to represent the adhesive matrix surrounding the fillers. Nevertheless, the fillers are taken into account implicitly because they have a catalytic effect on the reaction kinetics due to the OH groups on their surfaces. This can be seen from comparison of the relevant plots (middle panels in Figure 3 versus bottom panels). For DGEBA/IPD+FDC, the decrease of the A_1 and A_1' species and the increase of the A_2, A_2', A_3, and A_3' amines in the region from 0 to approximately 8 h is stronger than that for DGEBA/IPD. After this time, the beginning diffusion control slows down the reactions.

For DGEBA/IPD, the first structure model corresponding to a curing time of approximately 1.4 h is generated by formation of four bonds (creating one A_2 and three A_2' type cross-linking sites) according to the kinetic modeling based on the DSC data (see the top panels in Figure 3). For that purpose, an analysis of the structure is performed, and a list of distances of all epoxy oxygens to the nitrogens of the amine groups is generated, taking into account all 26 images of the periodic supercell. The one primary amine of the 1-amino groups closest to an epoxy ring is taken to form a secondary amine of the A_2 type (see Figure 2) and the three primary amines of the 3-aminomethyl groups closest to an epoxy ring are used to form secondary amines of the A_2' type. After formation of the new bonds, the corresponding force field parameters (atom, bond, angle, dihedral (torsion), and improper (out-of-plane) type) are adapted to the new bonding situation, and the combination of the *NVT* and *NpT* MD mentioned above is applied to equilibrate the new structure. In the same way, 11 further model structures of the adhesive during curing are generated step by step at various times with two to five new cross-links each. The last structure at 167 h = 6.9 d represents the final cured state of the adhesive with a total of 40 cross-links (10 A_3 and 10 A_3'), a degree of cross-linking of 91.0%, and an epoxy conversion of 87%. Several of these final structures are generated to improve statistics. The average density is $\rho = 1.106 \pm 0.003$ g/cm^3. This DGEBA/IPD system is used as a benchmark for the following simulation of the water sorption and volume swelling of the adhesive.

For DGEBA/IPD+FDC, the first structure model corresponding to a curing time of 1.1 h is generated by formation of four

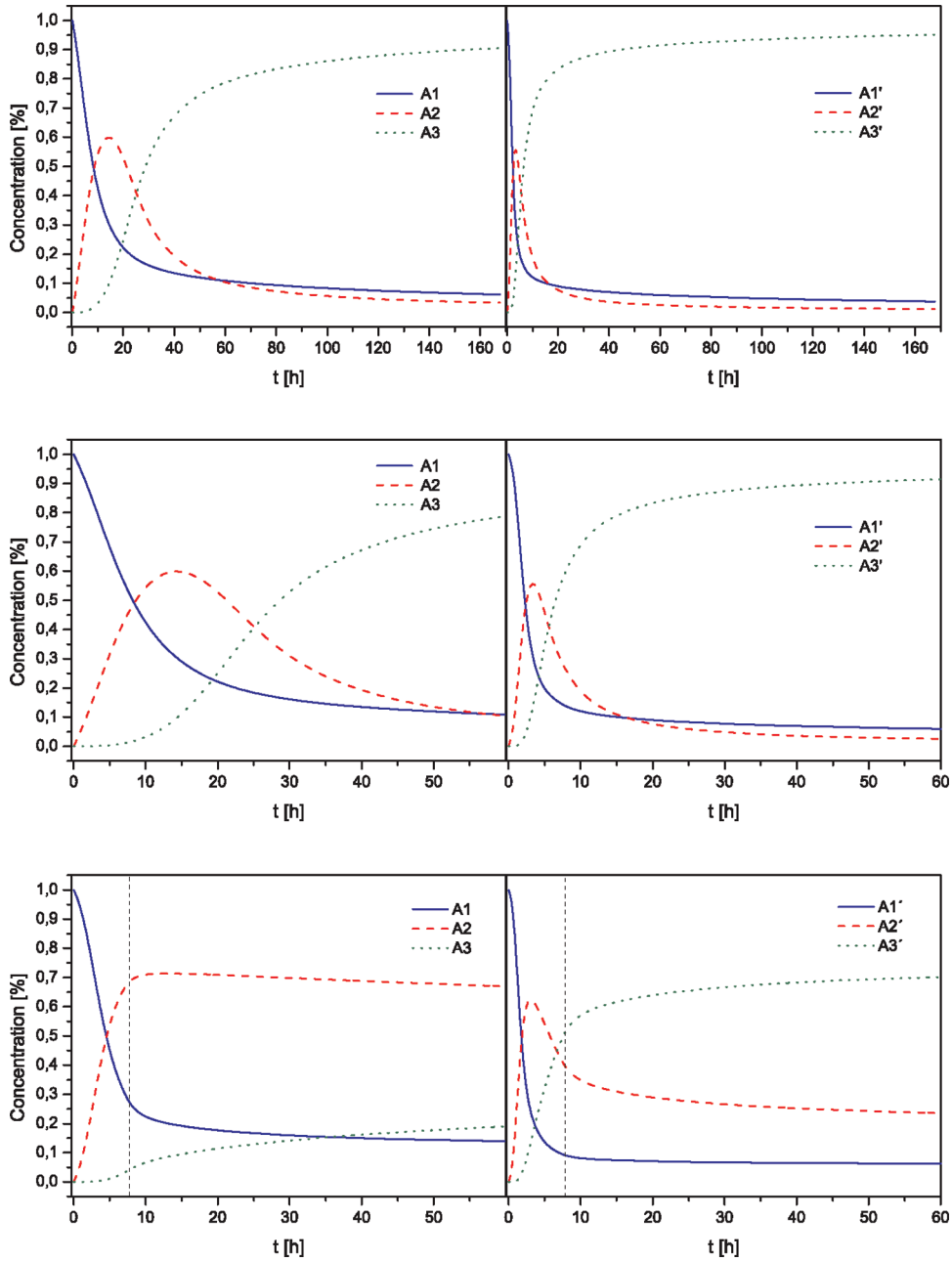

Figure 3. Concentrations of the species A_1, A_2, and A_3 (top left) and A_1', A_2', and A_3' (top right) versus time for 170 h and for the first 60 h (middle left and right) for DGEBA/IPD and for the first 60 h for DGEBA/IPD+FDC (bottom left and right). The dashed vertical line marks the beginning of the diffusion control.

bonds (creating one A_2 and three A_2' type cross-linking sites) according to the kinetic modeling (see the bottom panels in Figure 3). For the formation of the bonds, the structure is analyzed, and the corresponding distance list of all epoxy oxygens to the nitrogens of the amine groups is generated, taking into account the images of the periodic supercell. The corresponding amines closest to an epoxy ring are taken to form the secondary amines, and the corresponding force field parameters are adapted to the new bonding situation. Subsequently, the combination of the *NVT* and *NpT* MD mentioned above is applied to equilibrate the new structure. Eight further model structures of the adhesive during curing are generated step by step at various times with three to five new cross-links each. The last one at 759 h = 31.6 d represents the final cured state of the adhesive with a total of 35 cross-links (five A_2, two A_2', five A_3, and nine A_3'), a degree of cross-linking of 79.5%, and an epoxy conversion of 75%. For statistical reasons, several of these final structures are generated, and an average density of $\rho = 1.101 \pm 0.002$ g/cm^3 is obtained for the adhesive. Taking into account the fillers results in a total density of $\rho_{total} = 1.484$ g/cm^3, corresponding to a specific volume of $V_{spec} = 0.676$ mL/g. Mercury volume dilatometry measurements (2 weeks at 296 K) yield an experimental density of $\rho_{total,exp} = 1.495$ g/cm^3 and a specific volume of $V_{spec,exp} = 0.669$ mL/g for DGEBA/IPD+FDC. Thus, the simulation results are in very good agreement with the experimental data, showing a deviation of less than 1% in the density and around 1.1% in the specific volume. Hence, the generated models of DGEBA/IPD+FDC are considered realistic structure models of the investigated adhesive, and the system is used as basis for the following simulation of the water sorption and volume swelling of the real adhesive.

Wu and Xu,[14] who also investigated the DGEBA+IPD system, used a final conversion of 93.7% as criterion for

discontinuing the cross-linking. They obtained a density of 1.116 g/cm^3. This is found to be in good agreement with an experimental density of 1.131 g/cm^3 determined by Sindt et al.[62] and the corresponding elastic constants including the bulk, Young's, and shear modulus. In contrast to our approach, Wu and Xu used an exact stoichiometric mixture (16 DGEBA/8 IPD) instead of 23:11 used here, and no fillers were added. Additionally, Sindt et al. chose the curing schedule in order to obtain a maximum glass transition temperature of 436 K (heating from room temperature to 413 K at 2 K/min, 1 h at 413 K, then heating from 413 to 463 K at 2 K/min, and a final stay at 463 K for 6 h) instead of curing at 296 K, as in our case. An excess of epoxide is known to result in an increase of the degree of cross-linking and final conversion, but because the difference in the mixtures is very small, this effect can be neglected. The fillers have some catalytic effect on the reaction, as already discussed above. However, more important, curing at a definitely lower temperature results in a decrease of the final conversion and cross-linking. Hence, this results in a lower density, and thus, the density of 1.101 g/cm^3 obtained for the DGEBA/IPD+FDC system and the corresponding glass transition temperature of 335 K are also in reasonable agreement with the results of Sindt et al. and Wu and Xu.

III. Equilibrium Water Content

If a polymer network can exchange water molecules with another medium, for example, neat liquid water or air at a given relative humidity, there will be a net transfer of water molecules between the systems until the water content of the polymer network reaches an equilibrium value. At this water content, the chemical potential of water inside of the polymer matrix is identical to the chemical potential of water outside of the network. In this work, we determine the equilibrium water content of polymer networks by measuring the chemical potential of water inside of the polymer network for different water contents and comparing it to the chemical potential of water in neat water and air for different relative humidities at the same thermodynamic conditions.

It is favorable to use a rigid water model, that is, a model where the bond lengths and the angle between the bonds in the water molecule are fixed, when using the test particle insertion method to calculate the chemical potential of water. This is because the reduction of internal degrees of freedom of the test particles, compared to a flexible water model, reduces the computational cost of the method. In addition, molecular vibrations are difficult to include in a method based on classical statistical mechanics because molecular Debye temperatures usually are much higher than the temperatures of interest. During the MD simulations performed to estimate the equilibrium water contents, the bond lengths and angles of the water molecules in the systems are kept constant via the well-known SHAKE algorithm.[63]

The condition of chemical equilibrium of a species s distributed over two coexisting regions or phases, I and II, is $\mu_{s,I} = \mu_{s,II}$. Here, μ_s, the (classical) chemical potential of s, is given by $\mu_s = RT\ln(\rho_s\Lambda_T^3) + \mu_{s,rot} + \mu_{s,ex}$ in the case of rigid water models. The quantity ρ_s is the number density of s, Λ_T is the thermal wavelength of s, and $\mu_{s,rot}$ is the rotational chemical potential. This quantity is computed in the ideal gas limit and is therefore independent of the phase. Notice that the integration over the Euler angles is accounted for by a factor of $8\pi^2$, while the actual angular integration plus a factor $\sin(\theta)$, from the Jacobian of the transformation from the momenta conjugate to the Euler angles to angular velocities, become part of the evaluation of the excess chemical potential. Thus, $\mu_{s,rot,I} = \mu_{s,rot,II}$ and the condition of chemical equilibrium yields

$$RT\ln\left(\frac{\rho_{s,I}}{\rho_{s,II}}\right) = \mu_{s,ex,II} - \mu_{s,ex,I} \tag{1}$$

The most commonly used method for calculating the excess chemical potential is the test particle insertion method suggested by Widom[19] and independently by Jackson and Klein.[20] Calculating the excess chemical potential μ_{ex} in the *NPT* ensemble according to Widom's method yields[64]

$$\mu_{ex} = -RT\ln\left[\frac{1}{\langle V\rangle_{NPT}}\left\langle\frac{1}{8\pi^2}\int_V \mathrm{d}^3r\int_0^{2\pi}\mathrm{d}\phi\int_0^{\pi}\mathrm{d}\theta\sin\theta\times \int_0^{2\pi}\mathrm{d}\psi\,\exp[-\beta\Delta u(\vec{r},\phi,\theta,\psi)]\right\rangle_{NPT}\right] \tag{2}$$

Here, $\Delta u(\vec{r},\phi,\theta,\psi)$ is the potential energy of a virtual water molecule inserted into the system, consisting of polymer plus already present water. The position and orientation of the virtual water molecule are given by $\vec{r}$ and the Euler angles ϕ, θ, and ψ. T is the temperature ($\beta = (RT)^{-1}$) and V the volume of the system. The ensemble average in eq 2 is calculated by averaging over K configurations of the system produced during a *NPT* MD simulation. For each configuration, the integral in eq 2 is computed approximately by inserting a test water molecule M times into the system randomly and calculating its potential energy Δu, that is

$$\mu_{ex} = -RT\ln\left[\left(\sum_{k=1}^{K}V_k\right)^{-1}\left(\sum_{k=1}^{K}\frac{V_k}{M}\sum_{m=1}^{M}\exp[-\beta\Delta u_m]\right)\right] \tag{3}$$

To our knowledge, all rigid water models use the 12−6 Lennard-Jones (LJ) potential, $u(r) = C_{12}r^{-12} - C_6r^{-6}$, instead of the 9−6 LJ potential, $u(r) = C_9r^{-9} - C_6r^{-6}$, employed in the polymer consistent force field (PCFF). Here, we use a hybrid force field that uses the PCFF to describe the polymer and the interactions between polymer atoms and the simple point charge/extended[65] (SPC/E) water model to describe the water molecules and the interactions between different water molecules. LJ interactions between an atom in the polymer network and water are described by the 12−6 LJ potential. The LJ parameters of the polymer atoms in these interactions are taken from a third force field (cf. below). We use the particle−particle particle-mesh (PPPM) technique[66] to calculate the electrostatic interactions during the MD simulations and the standard Ewald summation[67] to calculate the Coulomb energy of the inserted test molecules during the calculation of the chemical potential.

For the MD simulations producing the configurations needed for the calculation of the chemical potential, we use the LAMMPS molecular dynamics software. The temperature and pressure inside of the simulation box are adjusted via the weak coupling method by Berendsen et al.[68] This method is numerically very stable, but the ensemble generated is not the desired *NPT* ensemble. Nevertheless, in our case, the effect on the chemical potential is small ($\mathcal{O}(N^{-1})$). After an equilibration phase, the positions of all atoms are stored at regular intervals for subsequent use in the calculation of the excess chemical potential.

Calculating the chemical potential at high densities directly from eq 3 yields prohibitively slow convergence. This is due to the exponential factor $\exp[-\beta\Delta u]$. If the molecule is inserted into an energetically favorable position/orientation, then Δu is either negative or a small positive number, and its contribution to the sum is relatively large. If the test molecule's potential energy is high, its contribution to the sum over $\exp[-\beta\Delta u]$ is vanishingly small. At high densities, a very small percentage of insertions is of the former type because there is a high probability that the inserted molecule will overlap with another particle in the box. The important contributions are the few ones which are inserted into "holes" large enough to contain a water molecule. In this work, we use an algorithm previously described in ref 21 to calculate the chemical potential more efficiently by focusing on these holes.

The simulation box is divided into $N_c \times N_c \times N_c$ cells of equal volume V_c. In each cell, we insert a test molecule at the center of the cell and calculate its potential energy. This is repeated for a total of 12 different orientations of the test molecule. If for at least one orientation the potential energy Δu satisfies

$$\exp[-\beta\Delta u] \geq \varepsilon \tag{4}$$

for a fixed value of the parameter ε, the cell is classified as a hole. Otherwise, the contribution of this cell to the chemical potential is neglected.

At this point, a subset of N_h of the original N_c^3 cells fulfills the condition (eq 4). Into each of the N_h cells, M_h test molecules are inserted at random positions and with random orientations and their potential energies are calculated. The excess chemical potential is now given by

$$\mu_{ex} = -RT\ln\left[\left(\sum_{k=1}^{K} V_k\right)^{-1}\left(\sum_{k=1}^{K}\frac{V_c}{M_h}\sum_{i=1}^{N_{h,k}}\sum_{m=1}^{M_h}\exp[-\beta\Delta u_m]\right)\right] \tag{5}$$

The influence of the parameters N_h and ε on the efficiency and quality of this method are discussed in ref 21. Notice, in particular, that this reference also contains extensive tests of the method for bulk water as well as a discussion of the effectiveness in comparison to the ordinary Widom method.

If the so-obtained chemical potential of water inside of the polymer network is lower than the chemical potential of water outside of the network, additional water molecules are inserted into the system. Suitable positions for these molecules are selected using the same algorithm used to find the holes in the configurations. From the list of N_h cells, we remove cells that are closer than 2.9 Å to another cell from the list in order to avoid inserting two water molecules too close to each other. The positions at which the new water molecules are inserted are chosen randomly from the remaining cells. With the new configuration, we repeat the MD simulations and the calculation of the chemical potential, compare it to the chemical potential of water outside of the network, and insert additional water if necessary. This process is repeated until the chemical potentials are equal.

In order to reduce systematical errors, we apply the procedure described above, starting from 10 different system configurations in parallel for both polymer systems, PA-6 and DGEBA+IPD. The statistical uncertainties of the chemical potential values are estimated by applying the bootstrap resampling method introduced by Efron[69] to the configurations used to calculate the chemical potentials. From the original set of K configurations, we create new sets of K configurations each by a random draw with replacement. We now compute the chemical potential for each of these new sets, that is, for each set, the summation over all configurations in eq 3 is now evaluated over all configurations in the respective set. Note that it is not necessary to repeat the computationally expensive summation over the insertions of test molecules for each configuration. The resulting distributions of the so-obtained values for the chemical potentials are, in general, quite complex and asymmetric. Therefore, we use confidence intervals as estimates of the statistical uncertainty of the chemical potential. The given confidence intervals are calculated by finding the smallest interval that contains the chemical potentials of the respective percentage of the resampled sets of configurations.

The method described thus far applies to a completely submerged polymer sample at a given temperature and pressure. In this case, we obtain the reference chemical potential of neat water at the same temperature and pressure as the polymer network using the same method as before. In addition, the result for liquid water can also be used to calculate the chemical potential of water in air at arbitrary relative humidity. At constant temperature, the difference in the chemical potential of a one-component system at two different pressures, P_0 and P_1, is given by

$$\mu(T,P_1) - \mu(T,P_0) = \int_{P_0}^{P_1} V_{mol}\,dP \tag{6}$$

where V_{mol} is the molar volume of water. Starting in the liquid phase, we follow an isotherm to the liquid−gas phase boundary, that is, $P_l(T) = P_v(T)$, where $P_v(T)$ is the vapor pressure of water at this temperature. Inside of the liquid phase, the molar volume of water is constant to very good approximation. The resulting change of the chemical potential in the liquid phase is small and can be neglected. If the relative humidity is φ, we continue along the isotherm until $P_{H_2O} = \varphi P_v$. Solving the integral in eq 6 assuming the ideal gas law yields

$$\mu(T,P,\varphi) - \mu(T,P,100\%) = RT\ln\varphi \tag{7}$$

Estimating chemical potentials via simulation is computationally expensive. Therefore, it is desirable to approximately determine the temperature dependence of the chemical potential via suitable thermodynamic relations. The derivative of the Gibbs−Helmholtz equation

$$\left.\frac{\partial(G/T)}{\partial T}\right|_{N,P} = -\frac{H}{T^2} \tag{8}$$

with respect to the number of water molecules inside of the polymer matrix, N_{H_2O}, yields a partial differential equation for the chemical potential of water inside of the polymer matrix, μ_{H_2O}, as a function of temperature and the number of water molecules.

$$\left.\frac{\partial(\mu_{H_2O}/T)}{\partial T}\right|_{\{N_i\},P} = -\frac{1}{T^2}\left.\frac{\partial H}{\partial N_{H_2O}}\right|_{\{N_i\}_{i\neq H_2O},P,T} \tag{9}$$

The algorithm for determining the equilibrium water content described above includes MD simulation of the polymer network at $T = T_0$ and different water contents N_{H_2O}. Calculating the

enthalpy $H = U + PV$ of the system during these simulations allows us to calculate the right-hand side of eq 9 for $T = T_0$ without additional computational cost. This yields the sign of $\partial\mu_{H_2O}/\partial T$ at $T = T_0$ and a rough approximation of μ_{H_2O} at other temperatures by assuming $\partial H/\partial N_{H_2O} \propto T^2$. Thus, the chemical potential of water inside of the polymer at temperature T_1 based on the chemical potential and enthalpy at temperature T_0 approximately is

$$\mu_{H_2O}(T_1, P) = \frac{T_1}{T_0}\left(\mu_{H_2O}(T_0, P) + \left(1 - \frac{T_1}{T_0}\right)\frac{\partial H}{\partial N_{H_2O}}\bigg|_{\{N_i\}_{i\neq H_2O}, P, T=T_0}\right) \quad (10)$$

Aside from the statistical error estimate discussed above, the Gibbs−Helmholtz equation may be used to independently obtain the potential energy per molecule, u, and thus provide an independent check. For a one-component system (bulk water), we have $u \approx -T^2\partial(\mu/T)/\partial T|_P - 3RT$. The last terms accounts for the kinetic energies of translation and rotation. Using the two bulk chemical potential values, $\mu = -13.34$ kcal mol^{-1} at $T = 300$ K and $\mu = -14.6$ kcal mol^{-1} at $T = 353$ K (cf. below), to estimate the derivative $((\partial\mu/T)/(\partial T))_P$, we obtain -7.2 kcal mol^{-1} for the mean potential energy per molecule. This is considerably less negative than the value of u directly obtained directly during MD, that is, $u \approx -11$ kcal mol^{-1}. However, if instead we use -13.6 and -14.35 kcal mol^{-1} (i.e., changes of ∓ 0.25 kcal mol^{-1}), we obtain -9.7 kcal mol^{-1}. This still is less negative than the above value. However, by using two temperature values 53 K apart, we have underestimated the slope at 300 K. To estimate the magnitude of this effect, we consider the experimental chemical potential versus temperature data in ref 21. The mean potential energy per molecule at $T = 300$ K, based on the slope computed using a second chemical potential at 353 K, is ~1.4 kcal mol^{-1} less negative than the value obtained via the exact derivative based on a second-order polynomial fit through the chemical potential data. This means that our above value, that is, -9.7 kcal mol^{-1}, can be considered consistent with the mean potential energy per particle obtain directly from the MD assuming chemical potential errors in the above range.

IV. Results: Swelling Simulations

Chemical Potential of Water. In order to find the equilibrium water content of the polymer, we need to know the chemical potential of water in the surrounding medium. We obtain the chemical potential of water in pure, liquid water at the same thermodynamic conditions using the same method as that for water inside of the polymer. We use configurations, extracted every 0.1 ps during a 2.5 ns MD simulation, containing 1000 SPC/E water molecules. The parameters used for the MD simulation of pure water are $\Delta t = 0.5$ fs, $\tau_T = 2$ ps, and $\tau_P/\kappa_T = 4.93 \times 10^6$ fs bar^{-1}. A $30 \times 30 \times 30$ grid with $\varepsilon = 0.5$ and 1000 insertions per hole is used in the calculation of the chemical potential with the accelerated Widom method.

PA-6. The molecular dynamics simulations of the PA-6 system with variable water content are carried out at $T = 300$ K and $P = 1$ bar with a time step Δt of 0.1 fs. We use the temperature relaxation time of $\tau_T = 1$ fs in the Berendsen thermostat and the coupling constant $\tau_P/\kappa_T = 1.97 \times 10^6$ fs bar^{-1} in the Berendsen barostat. The cutoff of the LJ interactions is 9 Å. For each water content and network configuration, the system is equilibrated for 100 ps, followed by a 0.5 ns simulation, during which the atomic positions are stored every 0.5 ps.

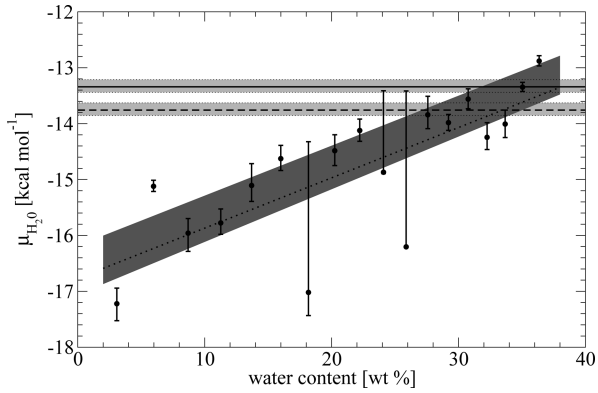

Figure 4. Chemical potential of water in PA-6 versus the water content at $T = 300$ K and $P = 1$ bar using the parameters from the Encad force field. The dotted line is a linear regression line through the data points. Dark shading indicates the area enclosed by linear regression lines through the upper and lower limits of the confidence intervals. The solid (dashed) horizontal line indicates the chemical potential of water in liquid water (in air at 50% relative humidity). The light shaded areas represent the statistical uncertainties.

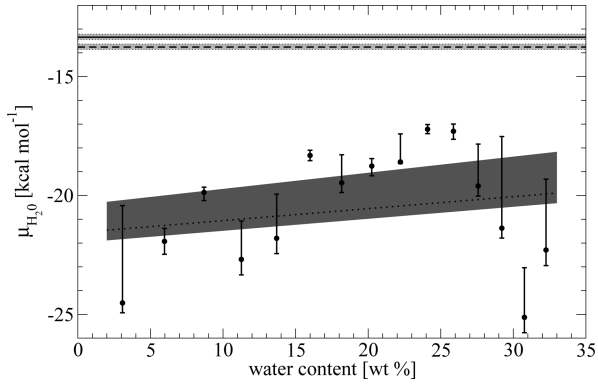

Figure 5. Chemical potential of water in PA-6 versus the water content at $T = 300$ K and $P = 1$ bar using the parameters from the Gromos force field. The meaning of symbols, line types, and shadings is the same as that in Figure 4.

The resulting 10000 network configurations for each water content are used to calculate the chemical potential using the improved Widom method described above. The parameters for the grid search are $\varepsilon = 0.1$ and $N_c = 25$. Into each cell classified as a hole, 2000 test molecules are inserted. The same value for ε is used in the search for suitable positions to insert additional water molecules into the system.

The results of the chemical potential measurements for PA-6 for which the missing LJ parameters of the polymer atoms in the LJ interactions between an atom in the polymer network and water are taken from the Encad[70] or Gromos 53a6 force field[71] are shown in Figures 4 and 5. The confidence intervals of the averages of the chemical potentials are calculated as described above. The equilibrium water content is estimated as the intersection of the linear regression line through the data points with the reference chemical potentials. Its error is estimated by the interval between the intersections of regression lines through the upper and lower limits of the confidence intervals and the reference chemical potential. With the Encad parameters, chemical equilibrium is observed at about 37 wt % water at 100% relative humidity and 33 wt % water at 50% relative humidity (cf. Table 1), which is significantly higher

TABLE 1: Simulated Equilibrium Water Content and Volume Swelling Ratio of PA-6 in Contact with Air at T = 300 K for 50 and 100% Relative Humidity

relative humidity	equilibrium water content	equilibrium volume swelling ratio
100%	37 wt % +1/−6	53% +2/−13
50%	33 wt % +2/−6	44% +5/−11

than expected from experimental results[72] showing equilibrium water contents at 100% relative humidity between 6 and 12 wt % depending on the crystallinity of the sample. Linear extrapolation based on these results yields an estimation of 15 wt % for the equilibrium water content of amorphous PA-6. The simulations using the LJ parameters from the Gromos force field reach no equilibrium and even show a decrease of the chemical potential at high water contents. At these high water contents, we observe in both cases a separation between the polyamide chain and the water molecules, which would explain the discrepancy. Taking into account only the calculated data for low water content, where no separation is observed, the linear regression yields an equilibrium water content of slightly above 20 wt % for the Encad parameters. This would be in reasonable agreement with the experiment. The volume swelling ratio, expressed as the percentage increase of the swollen network's volume compared to the volume of the dry network, can be found in Figure 6 and Table 1. The standard errors, $\sigma/\sqrt{n}$, of the data points are calculated from the root-mean-square deviation, σ, of the individual swelling ratios of the 10 simulated networks, which are assumed to be statistically independent, that is, $n = 10$.

The water content of amorphous PA-6 was also studied by Knopp and Suter, as mentioned in the Introduction.[29] Using an approach based on thermodynamic coupling parameter integration, they obtained water contents close to 20 vol. %, in good agreement with the experiment. We note that in ref 29, these authors erroneously state that the equality of the excess part of the chemical potential is used to find the equilibrium water content. However, in a private communication with one of the authors (U.S.), we learned that the actual calculations are based on the correct equality of the full chemical potential.

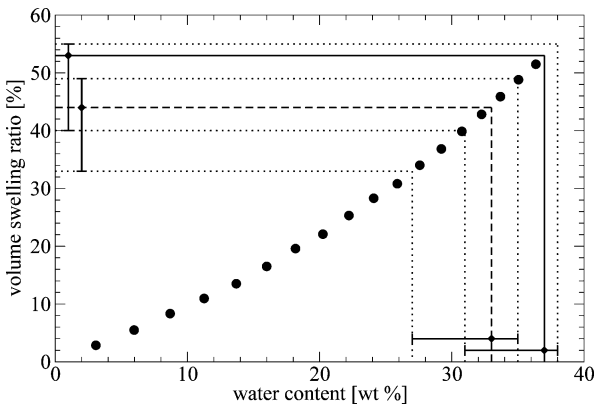

Figure 6. Volume swelling ratio of PA-6 versus the water content at T = 300 K and P = 1 bar using the parameters from the Encad force field. The diamonds indicate the equilibrium water contents and swelling ratios of the network in contact with air of 100 and 50% relative humidity. The solid line connects the volume swelling ratio with the observed equilibrium water content at 100% relative humidity, and the dashed line connects the corresponding equilibrium values in air at 50% relative humidity. Dotted lines represent the water content and swelling ratio at the limits of the confidence intervals. Standard errors are smaller than the symbols.

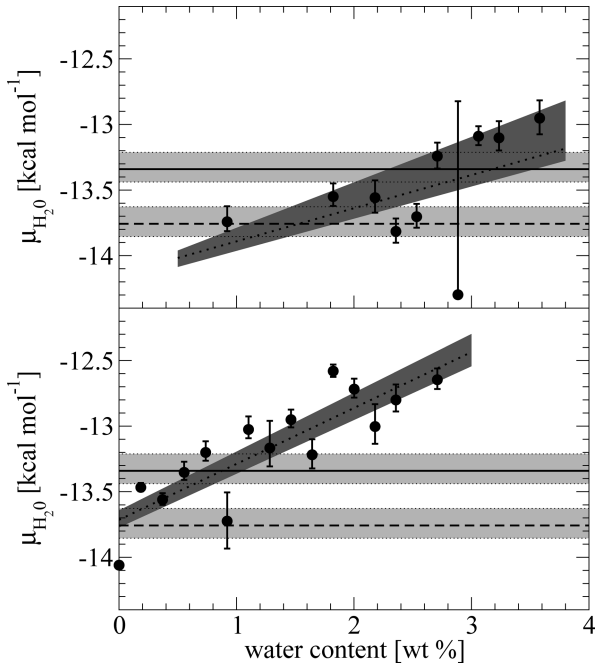

Figure 7. Top: Chemical potential of water in DGEBA/IPD versus the water content at T = 300 K and P = 1 bar using the parameters from the Encad force field. The meaning of symbols, line types, and shadings is the same as that in Figure 4. Bottom: Same as above, but for DGEBA/IPD+FDC.

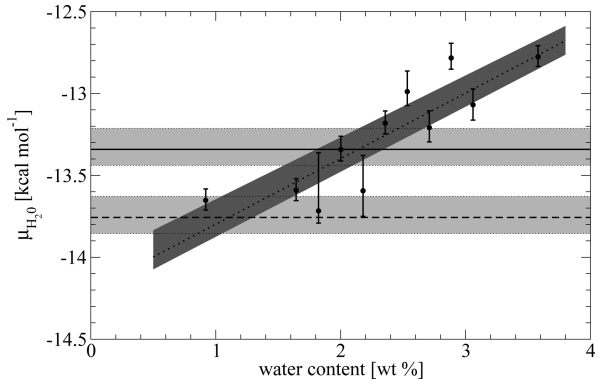

Figure 8. Chemical potential of water in DGEBA/IPD versus the water content at T = 300 K and P = 1 bar using the parameters from the Gromos force field. The meaning of symbols, line types, and shadings is the same as that in Figure 4.

DGEBA+IPD. For the DGEBA+IPD systems, we apply the same simulation scheme for the calculation of the equilibrium water content as that used previously for the PA-6 system. Simulation parameters which are different in this system include Δt = 0.5 fs, τ_T = 20 fs, and τ_P/κ_T = 1.97 × 10^5 fs bar^{-1}. Positions are stored every picosecond during a simulation of 1 ns after 100 ps of equilibration. The calculation of the chemical potentials is done using a 30 × 30 × 30 grid and 1000 insertions per hole.

The results are shown in Figures 7 and 8 and the observed equilibrium water contents are listed in Table 2. Experiments[73] show an equilibrium water content of 1.0 wt % at 50% relative humidity and 1.5 wt % at 95% relative humidity for a DGEBA+IPD system without fillers and with a similar degree of cross-linking as the DGEBA/IPD model. The results from the simulations for the DGEBA/IPD model at 1.5 wt % for the Encad force field and 1.1 wt % for the Gromos force field at 50% relative humidity and 3.2 wt % for the Encad force field and 2.1 wt % for the Gromos force field at 100% relative

TABLE 2: Simulated Equilibrium Water Content and Volume Swelling Ratio of DGEBA+IPD Systems in Contact with Air at $T = 300$ K for 50 and 100% Relative Humidity

relative humidity	system (force field)	equilibrium water content	volume swelling ratio
100%	DGEBA/IPD (ENCAD)	3.2 wt % +0.3/−1.0	2.35% +0.25/−1.15
	DGEBA/IPD (GROMOS)	2.1 wt % +0.2/−0.3	0.7% +0.2/−0.2
	DGEBA/IPD+FDC (ENCAD)	0.9 wt % +0.2/−0.2	0.65% +0.3/−0.1
50%	DGEBA/IPD (ENCAD)	1.5 wt % +0.3/−0.4	0.7% +0.4/−0.5
	DGEBA/IPD (GROMOS)	1.1 wt % +0.2/−0.4	0.2% +0.2/−0.2
	DGEBA/IPD+FDC (ENCAD)	<0.2 wt %	<0.1%

humidity are only slightly higher than the experimental results. On the basis of the results for the two test systems, PA-6 and DGEBA/IPD, we chose the Encad force field to be the best to provide the missing parameters in the pcff-SPC/E hybrid force field.

Figures 9 and 10 show the volume swelling ratio for the DGEBA+IPD systems as a function of the water content. Both sets of data for the DGEBA/IPD networks show the volume of the network to change only very little up to a water content of about 1 wt % and to grow linearly from thereon with increasing water content. This is probably due to existing cavities in the polymer network being filled by water before the network starts to expand. On the other hand, the DGEBA/IPD+FDC networks show a distinct increase in the network volume already at very low water contents. The equilibrium volume swelling ratio can be determined from this plot by looking at the swelling ratio belonging to the observed equilibrium water content. An estimate of the accuracy can be made from the swelling ratios that belong to the water contents at the limits of the confidence intervals. The results are listed in Table 2. Due to the small increase in volume for low water contents, the large uncertainties of the lower limits for the equilibrium water contents lead to even larger relative uncertainties for the lower limits of the equilibrium water contents.

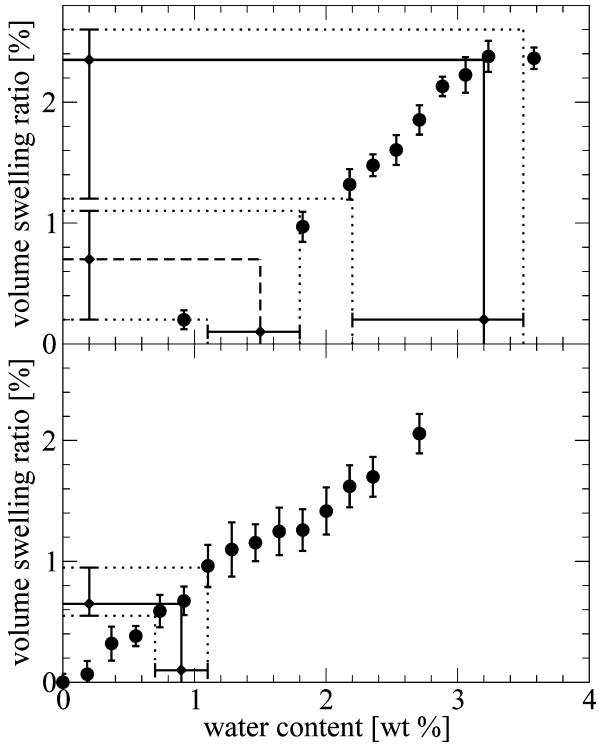

Figure 9. Top: Volume swelling ratio of DGEBA/IPD versus the water content at $T = 300$ K and $P = 1$ bar using the parameters from the Encad force field. The meaning of symbols and line types is the same as that in Figure 6. Bottom: Same as above, but for DGEBA/IPD+FDC.

The above results for the equilibrium water content and swelling ratio from the simulations of the DGEBA/IPD+FDC networks describe only the changes in the mass and volume of the polymer network and not the ones of the whole system of polymer and fillers. If we assume that the volume of the fillers is constant and that their effect on water sorption is negligible, we find an equilibrium water content of 0.51 ± 0.11 wt % and a volume swelling ratio of $0.49 + 0.23\%/-0.08\%$ for the adhesive. This result is in very good agreement with experiments[73] showing an equilibrium water content at 95% relative humidity between 0.45 and 0.6 wt %.

Chemical Potential at $T = 353$ K. As described above, we need the derivative of the system's enthalpy, H, with respect to the number of water molecules in the system, N_{H_2O}, in order to estimate the temperature behavior of the equilibrium water content. Figures 11 and 12 show the average enthalpy during the above simulations as a function of the number of water molecules for PA-6 and the DGEBA/IPD system. For both systems, the simulation results show a linear dependence on the number of water molecules. Thus, we assume $\partial H/\partial N_{H_2O}$ to be constant.

In order to test the quality of the approximation, we calculate the chemical potential of water in water and in both polymer systems for various water contents from computer simulations at $T = 353$ K. We use the final configurations from the simulations at $T = 300$ K as starting points for the simulations. Otherwise, the procedure and the parameters used in the calculation of the chemical potentials are the same as before. A comparison of the extrapolated results with the results from simulation is shown in Figure 13 for PA-6 and in Figure 14 for the DGEBA/IPD system. The equilibrium water contents obtained from this data using the same method as before are listed in Table 3. For the DGEBA/IPD system, the extrapolation overestimates the decrease of the chemical potential, which leads to a higher equilibrium water content

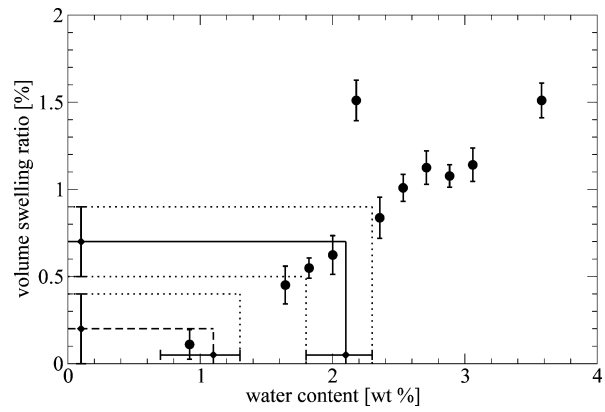

Figure 10. Volume swelling ratio of DGEBA/IPD versus the water content at $T = 300$ K and $P = 1$ bar using the parameters from the Gromos force field. The meaning of symbols and line types is the same as that in Figure 6.

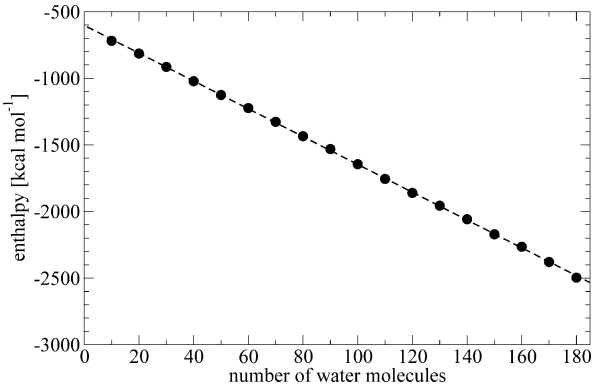

Figure 11. Enthalpy of PA-6 versus the water content at $T = 300$ K and $P = 1$ bar. The data points are the average enthalpies for the respective number of water molecules in the system calculated from the MD simulations. The dashed line is a linear fit to the data. Here and in the next figure, kcal mol^{-1} refers to moles of particles, whereas in all of the other figures, this unit refers to moles of water.

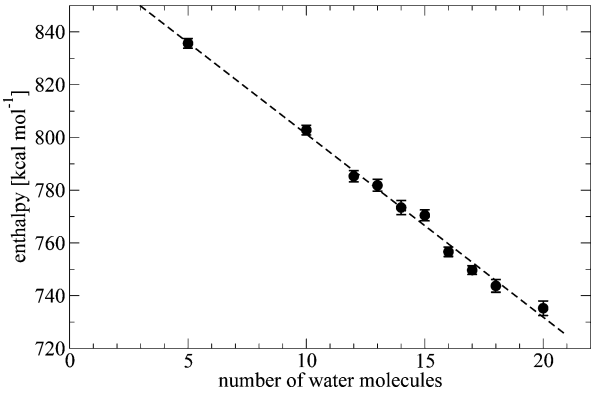

Figure 12. Enthalpy of DGEBA/IPD versus the water content at $T = 300$ K and $P = 1$ bar. The symbols are the same as those in Figure 11.

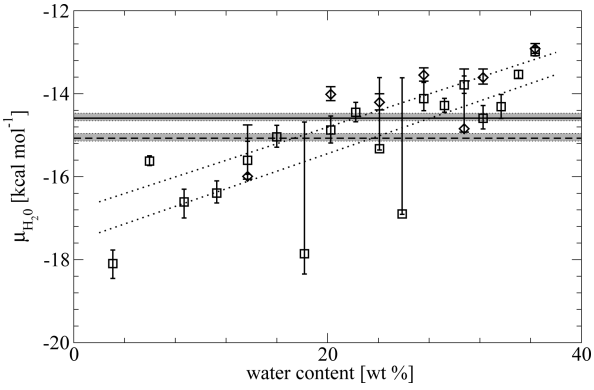

Figure 13. Chemical potential of water in PA-6 versus the water content at $T = 353$ K and $P = 1$ bar using the parameters from the Encad force field. The squares represent the chemical potentials extrapolated from the results at $T = 300$ K, and the diamonds represent the chemical potentials calculated directly from simulations at $T = 353$ K. The dotted lines are linear fits to the data sets. The solid (dashed) horizontal line indicates the chemical potential of water in liquid water (in air at 50% relative humidity). The light shaded areas represent the statistical uncertainties.

due to the small slope of the curve. In the case of PA-6, the extrapolated results show good agreement with the results from simulation within their error bars. Both systems show a decrease in the equilibrium water content with rising temperature.

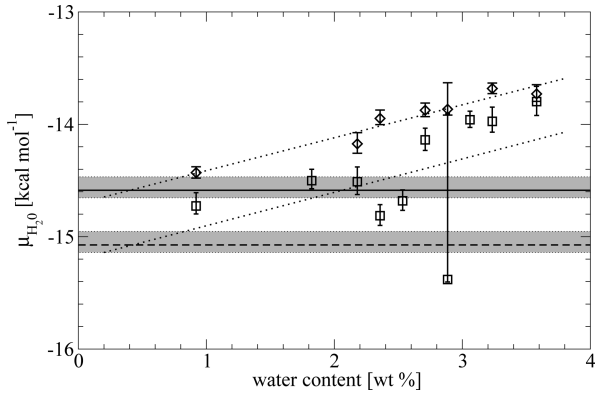

Figure 14. Chemical potential of water in DGEBA/IPD versus the water content at $T = 353$ K and $P = 1$ bar using the parameters from the Encad force field. The meaning of symbols and line types is the same as that in Figure 13.

TABLE 3: Simulated Equilibrium Water Content of DGEBA/IPD+FDC and PA-6 in Contact with Air at $T = 353$ K for 50 and 100% Relative Humidity

		equilibrium water content	
system	relative humidity	extrapolated	from simulation
DGEBA/IPD	100%	2.0 wt % +0.4/−0.5	0.4 wt % +0.1/−0.1
	50%	0.4 wt % +0.2/−0.2	<0.4 wt %
PA-6	100%	28 wt % +2/−6	23.5 wt % +2/−6
	50%	22 wt % +2/−8	17.5 wt % +1/−9.5

V. Conclusion

Atomistic model structures of amorphous PA-6 and of an adhesive system consisting of DGEBA and IPD are generated. In the case of the adhesive, a new approach for the construction of the cross-linked polymer network is introduced, taking into account the chemical reactivity of the adhesive's reactive species on the atomic level. Therefore, a combination of a kinetic model based on data obtained from thermal analysis and a force-field-based MD method is applied. With this approach, atomistic model structures can be generated for any desired curing time. The cross-linking is thereby based on the reaction kinetics including autocatalysis, diffusion control, and filler effects instead of using a distance criterion as in current state-of-the-art approaches. The degree of cross-linking and the epoxy conversion of the model structures of the adhesive with fillers (taking into account diffusion control and catalytic effect of the fillers) are intrinsically identical to the experimental data of the system. Furthermore, the density and glass transition temperature are found to be in good agreement with our own experimental data and the results of Sindt et al.[62] and Wu and Xu.[14] Thus, the new approach results in more realistic structure models with regard to the kind and number of cross-linking species formed on the atomic level. This is thought to be imperative for the calculation of volume shrinkage, water sorption, and volume swelling.

A previous approach to compute the chemical potentials of small molecules in dense systems is extended and applied to PA-6, as a test case, and the adhesive system DGEBA+IPD. In both cases, we determine the equilibrium water content and swelling at variable ambient conditions. We find that the use of the Encad force field in conjunction with the approach for the preparation of the polymer systems produces results in reasonable agreement with experiment. Therefore, the method put forward in this paper should certainly be interesting for many related systems for which the uptake of small molecules, water, in particular, affects their technical performance.

Acknowledgment. This work was supported through a grant from the German Federal Ministry of Education and Research (BMBF, Grant No.: 03 × 0502). We are also grateful to Jens Koschel (Sartorius AG), Jana Kolbe (Fraunhofer IFAM), Karsten Maenz (Carl Zeiss Jena GmbH), and Enno Oyen (Bergische Universität Wuppertal) for a number of helpful discussions.

References and Notes

(1) Theodorou, D. N.; Suter, U. W. *Macromolecules* **1985**, *18*, 1467–1478.
(2) Gelin, B. R. *Molecular Modeling of Polymer Structures and Properties*; Hanser Publishers: Munich, Germany, 1994.
(3) Binder, K. (Ed.) *Monte Carlo and molecular dynamics simulations in polymer science*, Oxford University Press, Oxford, U.K., 1995.
(4) Kremer, K. *Comput. Mater. Sci.* **1998**, *10*, 168–174.
(5) Hofmann, D.; Fritz, L.; Ulbrich, J.; Paul, D. *Comput. Theor. Polym. Sci.* **2000**, *10*, 419–436.
(6) Hofmann, D.; Fritz, L.; Ulbrich, J.; Schepers, C.; Böhning, M. *Macromol. Theory Simul.* **2000**, *9*, 293–327.
(7) Kotelyanskii, M.; Theodorou, D. N. *Simulation Methods for Polymers*; Marcel-Dekker: New York, 2004.
(8) Chern, C. S.; Poehlein, G. W. *Polym. Eng. Sci.* **1987**, *27*, 788–795.
(9) Wise, C. W.; Cook, W. D.; Goodwin, A. A. *Polymer* **1997**, *38*, 3251–3261.
(10) Cheng, K. C. *J. Polym. Sci., Part B: Polym. Phys.* **1998**, *36*, 2339–2348.
(11) Colin, X.; Marais, C.; Verdu, J. *Polym. Degrad. Stab.* **2002**, *78*, 545–553.
(12) Wu, S.; Soucek, M. D. *Polymer* **1998**, *39*, 5747–5759.
(13) Yarovsky, I.; Evans, E. *Polymer* **2002**, *43*, 963–969.
(14) Wu, C.; Xu, W. *Polymer* **2006**, *47*, 6004–6009.
(15) Wu, C.; Xu, W. *Polymer* **2006**, *48*, 5440–5448.
(16) Fan, H. B.; Yuen, M. M. F. *Polymer* **2007**, *48*, 2174–2178.
(17) Varshney, V.; Patnaik, S. S.; Roy, A. K.; Farmer, B. L. *Macromolecules* **2008**, *41*, 6837–6842.
(18) Clancy, T. C.; Frankland, S. J. V.; Hinkley, J. A.; Gates, T. S. *Polymer* **2009**, *50*, 2736–2742.
(19) Widom, B. *J. Chem. Phys.* **1963**, *39*, 2808–2812.
(20) Jackson, J. L.; Klein, L. S. *Phys. Fluids* **1964**, *7*, 228–231.
(21) Dömötör, G.; Hentschke, R. *J. Phys. Chem. B* **2004**, *108*, 2413–2417.
(22) Dömötör, G.; Hentschke, R. *Macromol. Theory Simul.* **2004**, *13*, 506–511.
(23) Pandiyan, S.; Brown, D.; Neyertz, S.; van der Vegt, N. F. A. *Macromolecules* **2010**, *43*, 2605–2621.
(24) Deitrick, G. L.; Scriven, L. E.; Davis, H. T. *J. Chem. Phys.* **1989**, *90*, 2370–2385.
(25) Tamai, Y.; Tanaka, H.; Nakanishi, K. *Macromolecules* **1995**, *28*, 2544–2554.
(26) Fukuda, M. *J. Chem. Phys.* **2000**, *112*, 478–486.
(27) Zanuy, D.; Alemán, C.; López-Carrasquero, F.; Báez, M. E.; García-Alvarez, M.; Laso, M.; Muñoz-Guerra, S. *Macromol. Chem. Phys.* **2001**, *202*, 564–573.
(28) Knopp, B.; Suter, U. W.; Gusev, A. A. *Macromolecules* **1997**, *30*, 6107–6113.
(29) Knopp, B.; Suter, U. W. *Macromolecules* **1997**, *30*, 6114–6119.
(30) Nick, B.; Suter, U. W. *Comput. Theor. Polym. Sci.* **2001**, *11*, 49–55.
(31) van der Vegt, N. F. A.; Briels, W. J. *J. Chem. Phys.* **1998**, *109*, 7578–7582.
(32) Müller-Plathe, F. *Macromolecules* **1991**, *24*, 6475–6479.
(33) Lim, S. Y.; Tsotsis, T. T.; Sahimi, M. *J. Chem. Phys.* **2003**, *119*, 496–504.
(34) Lu, Z. Y.; Hentschke, R. *Phys. Rev. E* **2001**, *63*, 051801.
(35) Lu, Z. Y.; Hentschke, R. *Phys. Rev. E* **2002**, *65*, 041807.
(36) Lu, Z. Y.; Hentschke, R. *Phys. Rev. E* **2002**, *66*, 041803.
(37) Lu, Z. Y.; Hentschke, R. *Phys. Rev. E* **2003**, *67*, 061807.
(38) Oyen, E.; Hentschke, R. *J. Chem. Phys.* **2005**, *123*, 054902.
(39) Hörstermann, H.; Hentschke, R. *J. Chem. Phys.* **2008**, *128*, 084902.
(40) Aydt, E. M.; Hentschke, R. *J. Chem. Phys.* **2000**, *112*, 5480–5487.
(41) de Pablo, J. J.; Laso, M.; Suter, U. W. *Macromolecules* **1993**, *26*, 6180–6183.
(42) Sommer, J. U.; Vilgis, T. A.; Heinrich, G. *J. Chem. Phys.* **1994**, *100*, 9181–9191.
(43) Trautenberg, H. L.; Sommer, J. U.; Görlitz, D. *J. Chem. Soc., Faraday Trans.* **1995**, *91*, 2649–2653.
(44) Kenkare, N. R.; Hall, C. K.; Khan, S. A. *J. Chem. Phys.* **2000**, *113*, 404–418.
(45) *Materials Studio Release Notes, Release 4.4*; Accelrys Software Inc.: San Diego, CA, 2008.
(46) Hagler, A. T.; Lifson, S.; Dauber, P. *J. Am. Chem. Soc.* **1979**, *101*, 5122.
(47) Hagler, A. T.; Lifson, S.; Dauber, P. *J. Am. Chem. Soc.* **1979**, *101*, 5133.
(48) Dauber-Osguthorpe, P.; Roberts, V. A.; Osguthorpe, D. J.; Wolff, J.; Genest, M.; Hagler, A. T. *Proteins: Struct., Funct., Genet.* **1986**, *4*, 82.
(49) Maple, J. A.; Hwang, M. J.; Stockfisch, T. P.; Dinur, U.; Waldman, M.; Ewig, C. S.; Hagler, A. T. *J. Comput. Chem.* **1994**, *15*, 162.
(50) Sun, H.; Mumby, S. J.; Maple, J. R.; Hagler, A. T. *J. Am. Chem. Soc.* **1994**, *116*, 2978.
(51) Sun, H.; Mumby, S. J.; Maple, J. R.; Hagler, A. T. *J. Chem. Phys.* **1995**, *99*, 5873.
(52) Sun, H. *Macromolecules* **1995**, *28*, 701.
(53) Plimpton, S. J. *J. Comput. Phys.* **1995**, *117*, 1–19.
(54) LAMMPS Molecular Dynamics Simulator. http://lammps.sandia.gov (accessed May 21, 2008).
(55) Hentschke, R.; Oyen, E. *J. Chem. Phys.* **2005**, *122*, 104904.
(56) Hoover, W. G. *Phys. Rev. A* **1985**, *31*, 1695.
(57) Hoover, W. G. *Phys. Rev. A* **1986**, *34*, 2499.
(58) Sourour, S.; Kamal, M. R. *Thermochim. Acta* **1976**, *14*, 41–59.
(59) Flammersheim, H. J.; Opfermann, J. *Thermochim. Acta* **1999**, *337*, 141–148.
(60) Opfermann, J. *J. Therm. Anal. Calorim.* **2000**, *60*, 641–658.
(61) Kolbe, J.; Wirts-Rütters, M.; Amkreutz, M.; Hoffmann, M.; Nagel, C.; Knaack, R.; Schneider, B. *Adhaes. Kleben Dichten* **2009**, *09*, 38–42.
(62) Sindt, O.; Perez, J.; Gerard, J. F. *Polymer* **1996**, *37*, 2989–2997.
(63) Ryckaert, J. P.; Ciccotti, G.; Berendsen, H. J. C. *J. Comput. Phys.* **1997**, *23*, 327–341.
(64) Shing, K. S.; Chung, S. T. *J. Phys. Chem.* **1987**, *91*, 1674–1681.
(65) Berendsen, H. J. C.; Grigera, J. R.; Straatsma, T. P. *J. Phys. Chem.* **1987**, *91*, 6269–6271.
(66) Hockney, R. W.; Eastwood, J. W. *Computer Simulations using Particles*; Adam Hilger: New York, 1989.
(67) Ewald, P. P. *Ann. Phys.* **1921**, *369*, 253–287.
(68) Berendsen, H. J. C.; Postma, J. P. M.; van Gunsteren, W. F.; DiNola, A.; Haak, J. R. *J. Chem. Phys.* **1984**, *81*, 3684.
(69) Efron, B. *Ann. Stat.* **1979**, *7*, 1–26.
(70) Levitt, M.; Hirshberg, M.; Sharon, R.; Daggett, V. *Comput. Phys. Commun.* **1995**, *91*, 215–231.
(71) Oostenbrink, C.; Villa, A.; Mark, A. E.; Van Gunsteren, W. F. *J. Comput. Chem.* **2004**, *25*, 1656–1676.
(72) Vieweg, R.; Müller, A. C. *Kunststoff-Handbuch, Bd. VI Polyamide*; Hanser Verlag: München, Germany, 1966.
(73) Eger, M.; Koschel, J.; Sartorius AG. Göttingen, unpublished results.

JP105210Y